TECHNICAL MEMORANDUM

16

Two case comparisons between vertical motions obtained from the quasi-geostrophic omega equation and those in the ECMWF analysis system

G.J. Cats and M.S. Tracton

Research Department

1980

European Centre for Medium-Range Weather Forecasts
Europäisches Zentrum für mittelfristige Wettervorhersage
Centre européen pour les prévisions météorologiques à moyen

Abstract

A computer program for solving the quasi geostrophic omega-equation available from NMC has been modified for use at ECMWF. In two test cases the vertical velocity obtained with this program shows, in the lower atmospheric layers, very good agreement with the vertical velocity in the initialised and first-guess fields, but not with the vertical velocity in the analysis field. Above 300 mbar both the results of the omega-equation and those of the initialised fields appear unrealistic. The separate contributions of the different terms in the omega-equation, the tendencies derived with the quasi-geostrophic vorticity equation and derived precipitation rates are shown.

1. INTRODUCTION

In weather prediction the vertical velocity in the atmosphere plays an important role, not only because it triggers rain fall and latent heat release, but also because of its effect on air parcel trajectories.

The continuity equation relates the vertical velocity to the divergence of the horizontal wind. Due to the wind observation errors, however, the vertical velocity cannot be derived from the observations directly, as follows from a simple order of magnitude estimate (Holton, 1972). Instead, the omega-equation is solved, which relates the vertical velocity, ω, in a pressure coordinate system to horizontal and vertical derivatives of well-observed quantities.

Recently a non-linear normal mode initialisation has been introduced (Temperton, 1979), which effectively reduces the divergent wind component by eliminating the growth of the gravity waves. After the application of this technique, the divergence should lead to the right order of magnitude for the vertical velocity by direct application of the continuity equation.

Tracton, (1978) wrote a computer program to solve the omega-equation. This paper describes two comparisons between the vertical velocity obtained with this program and those that follow from the initialised wind field. In Section 2 the omega-equation and the procedure to solve it are discussed. The third and fourth Section describe the comparison cases. A short description of the ECMWF version of the computer program follows in the Appendix.

2. THE OMEGA-EQUATION, ITS NUMERICAL SOLUTION AND SOME APPLICATIONS

2.1 The equations

The quasi-geostrophic omega-equation reads (Holton, 1972):

$$\underset{\sim}{\nabla}^2 \sigma_o \omega + f_o^2 \frac{\partial^2 \omega}{\partial p^2} = F \tag{1}$$

where ω is the vertical velocity in pressure coordinates, $\omega = \frac{dp}{dt}$, σ_o the static stability $\sigma_o = \frac{\alpha}{\theta} \frac{\partial \theta}{\partial p}$ (α being the specific volume and θ the potential temperature), f_o is the area average value of the Coriolis parameter f and F is the forcing, which consists of three terms:

$$F = F_\zeta + F_\theta + F_H \tag{2}$$

The differential vorticity advection F_ζ is given by

$$F_\zeta = -f_o \frac{\partial}{\partial p} \underset{\sim}{v}_g \cdot \underset{\sim}{\nabla} (\zeta_g + f) \tag{3}$$

In Equation (2) F_θ and F_H are proportional to the Laplacian of temperature advection and diabatic heat release, respectively:

$$F_\theta = - \underset{\sim}{\nabla}^2 (\underset{\sim}{v}_g \cdot \underset{\sim}{\nabla} \frac{\partial \Phi}{\partial p}) \tag{4}$$

$$F_H = - R/(C_p p) \underset{\sim}{\nabla}^2 H \tag{5}$$

In Equation (4), $\Phi = gz$ is the geopotential, from which the geostrophic velocity $\underset{\sim}{v}_g$ and vorticity ζ_g follow by $\underset{\sim}{v}_g = f_o^{-1}\ \underset{\sim}{k} \times \underset{\sim}{\nabla} \Phi$ and $\zeta_g = f_o^{-1}\ \underset{\sim}{\nabla}^2 \Phi$ respectively.

The boundary conditions to Equation (1) are $\omega = 0$ at $p = 0$ and, at the surface,

$$\omega_s = \omega_f + \omega_t \tag{6}$$

where the frictional part is given by (Holton, 1972)

$$\omega_f = \rho_s g\ f^{-1}\ \underset{\sim}{k} \times \underset{\sim}{\nabla}\ C_D\ v_s\ \underset{\sim}{v}_s \tag{7}$$

The surface topography induces

$$\omega_t = \rho_s \, g \, \underset{\sim}{v}_s \cdot \underset{\sim}{\nabla} z_s \qquad (8)$$

The symbols used denote the surface drag coefficient (C_D), the surface wind ($\underset{\sim}{v}_s$), the terrain height (z_s) and the density of the air at the surface (ρ_s).

In the derivation of Equation (1) some approximations have been made, such as the replacement of the advection velocity by the geostrophic velocity. The resulting set of equations expresses ω in terms of the height fields, the static stability σ_o and the diabatic heating H.

2.2 The procedure to solve the equations

Equations (1) to (8) are solved in two steps. At first, the diabatic heat release H is set to zero, and Equation (1) through (8) are integrated, such that the contributions of F_ζ, F_θ, ω_f and ω_t (see Equations (2) and (6)) are found separately. Then, in those areas where the total vertical velocity has been found to be upward ($\omega < 0$) in the first step, condensation is assumed to occur if the local relative humidity h exceeds a specified saturation value h_s. The associated latent heat release

$$H_L = - L \, \omega \, \frac{dQ_s}{dp} \qquad (9)$$

is used as an approximation to H in Equation (5). The material derivative of the saturation specific humidity dQ_s/dp is replaced by the local derivative $\frac{\partial Q_s}{\partial p}$.

According to Equations (5) and (9) F_H is proportional to $\underset{\sim}{\nabla}^2 \omega$ in condensation areas. Therefore Equation (1) can be written as

$$\underset{\sim}{\nabla}^2 \sigma_m \omega + f_o^2 \frac{\partial^2 \omega}{\partial p^2} = F_\zeta + F_\theta \qquad (10)$$

with $\sigma_m = \sigma_o - RL/(C_p p) \frac{\partial Q_s}{\partial p}$ in regions with condensation and $\sigma_m = \sigma_o$ elsewhere. Latent heat release therefore reduces static stability and enhances vertical motions (if upward). This enhancement is calculated as the difference between the solutions to Equations (1) and (10).

The computer program to solve the omega-equation (Tracton, 1978) uses as input the height of and the temperature and relative humidity at the standard pressure levels up to 100 mbar inclusive. These are interpolated by quadratic approximations to 10 levels with 100 mbar spacing from 1000 mbar to 100 mbar. The horizontal grid is 31 x 31 with arbitrary grid length. The dry static stability is taken to be the standard atmosphere values, depending on pressure only. The upper and lower boundaries of the region are replaced by the 1000 mbar and 100 mbar levels. Derivatives are replaced by centered finite differences and Equations (1) and (10), which are elliptic, are solved by an extrapolated Liebman relaxation scheme. Because the outer arrays of the grid points are lost in the finite differencing, only the results at the inner 25 x 25 grid are output on each computational level.

Only the input height fields are used to calculate the terms F_ζ, F_θ, ω_f and ω_t in Equations (2) and (6). The surface wind $\underset{\sim}{v}_s$ with components u_s, v_s is obtained from the 1000 mbar geostrophic wind components, u_g, v_g as

$$u = \alpha(\cos\theta \; u_g - \sin\theta \; v_g)$$
$$v = \alpha(\cos\theta \; v_g + \sin\theta \; u_g) \qquad (11)$$

with $\alpha = 0.67$ and $\theta = 23^o$

The surface drag is taken constant

$$C_D = 6.8 \; 10^{-4} \qquad (12)$$

The surface topography z_s is the smoothed ECMWF's N48 topography. If z_s exceeds the standard height of a level p, no condensation is allowed to occur within the 100 mbar layer centered around p. The relative humidity h and temperature input are used to check if h exceeds its saturation value h_s, which in the case study that follows has been taken to be 80%.

2.3 Some applications

The solution of the omega-equation can be used in the calculation of a number of important meteorological quantities. In this subsection the quantities that are calculated by the available programs are mentioned and an indication is given of the assumptions made. Full details can be found in Tracton, 1978.

1. Large scale precipitation is calculated from the vertical velocity under the assumption that all condensed water is precipitated out.

2. With the quasi-geostrophic vorticity equation (Holton, 1972) the geopotential tendencies are calculated.

3. The vertical fluxes of energy are calculated, as are the generation of kinetic energy and conversion of available potential to kinetic energy.

3. CASE STUDY 1

3.1 The situation

For one case the vertical velocity obtained with the omega-equation was compared to the vertical velocity resulting from the first-guess, the analysis and the initialised fields. The case chosen is 15 January 1979, 1200 UT. (FGGE experiment "IA").

The calculations were carried out over the area as shown in Fig. 1. The horizontal grid distance was 200 km at 60°N, which corresponds to the resolution of the used ECMWF model (N48). In Fig. 1 further the first-guess (6 hours forecast) 1000 mbar height field is shown. The analysis (Fig. 2) shows that the centre pressure of the low over Iceland was predicted a little too high. In this region the initialisation (Fig. 3) introduces minor changes. Similar statements hold for the 500 mbar height (Figs. 4, 5, and 6). The thickness chart (Fig. 7, derived from the initialised fields) indicates the position of the warm sector of the frontal system associated with the low. In Fig. 8 the geostrophic absolute vorticity $\zeta_g + f$ at 500 mbar and in Fig. 9 the relative humidity at 1000 mbar are shown after initialisation. (Due to the interpolation between the 25 x 25 grid some points seem to have relative humidities in excess of 100%). The high relative humidity also identifies the warm sector.

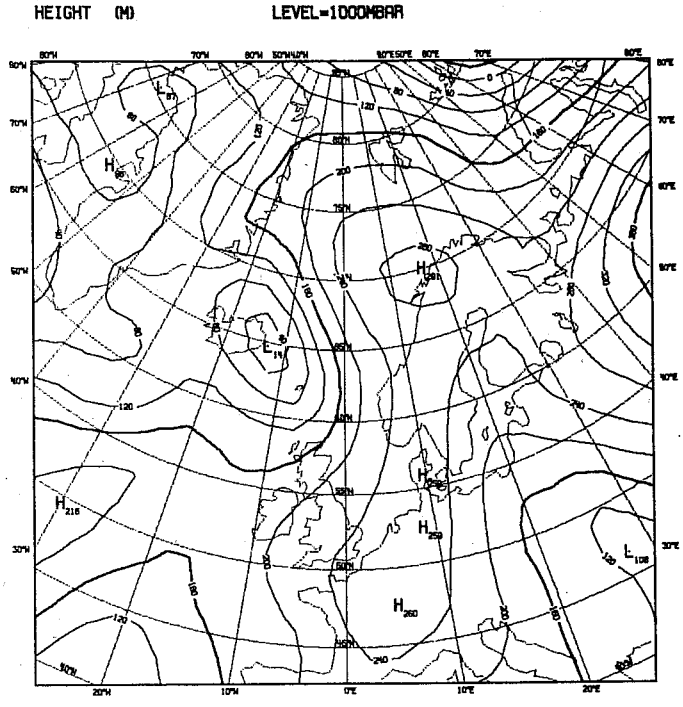

Fig. 1 First-guess height field of the 1000 mbar level, 15 January 1979, 1200 UT.

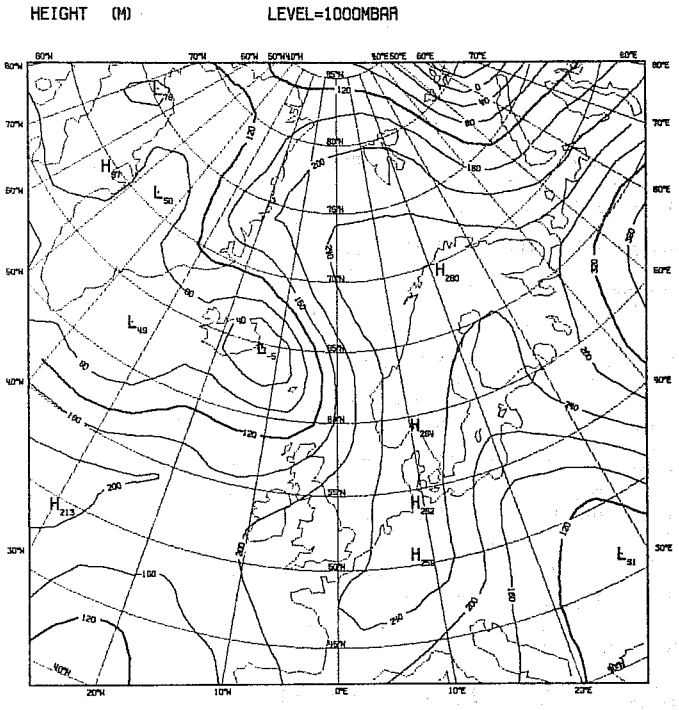

Fig. 2 As Fig. 1, however, analysed height field

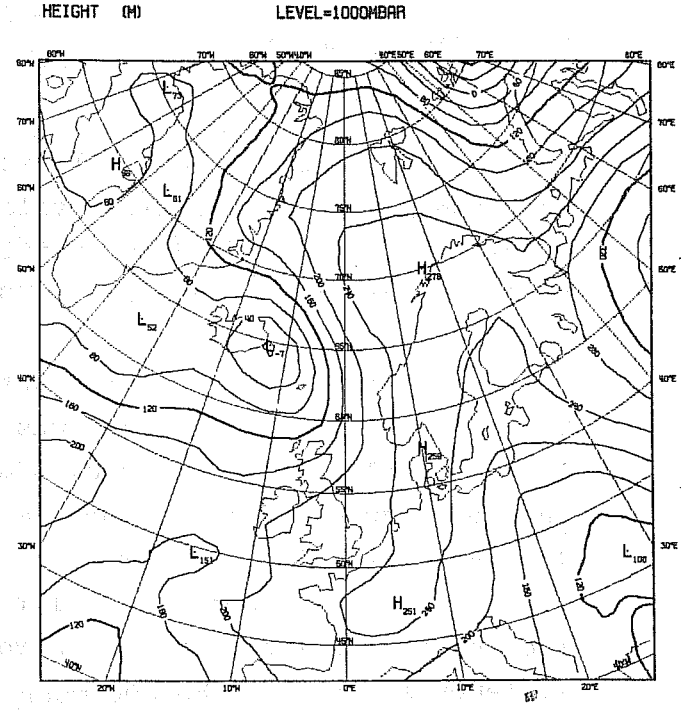

Fig. 3 As Fig. 1, however, initialised height field

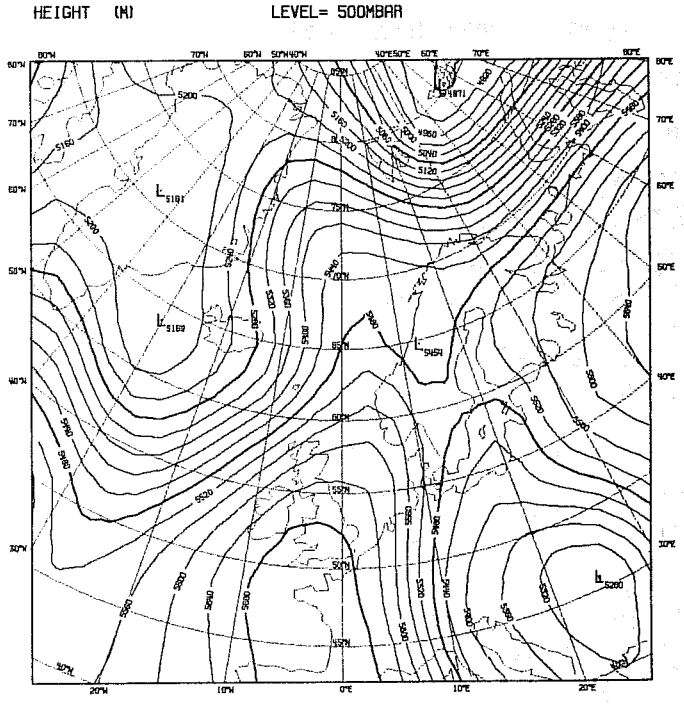

Fig. 4 First-guess 500 mbar height field

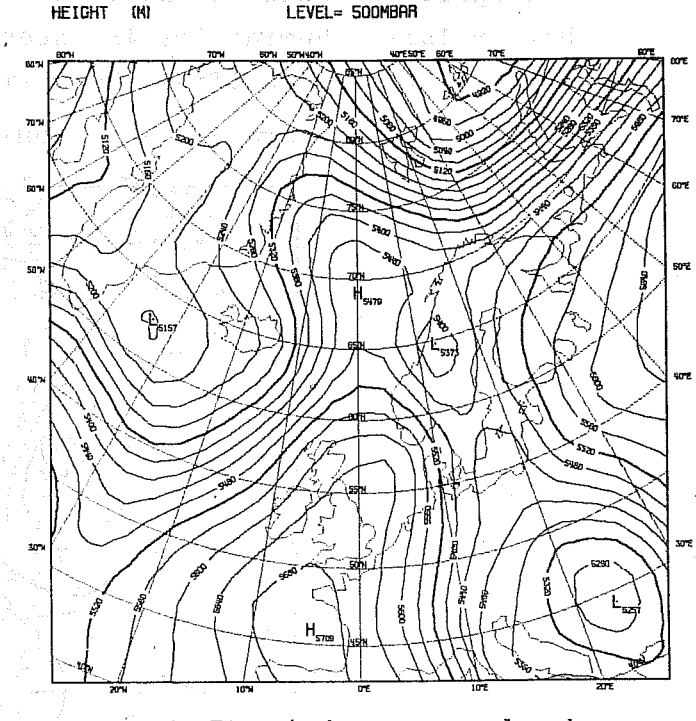

Fig. 5 As Fig. 4, however, analysed height field

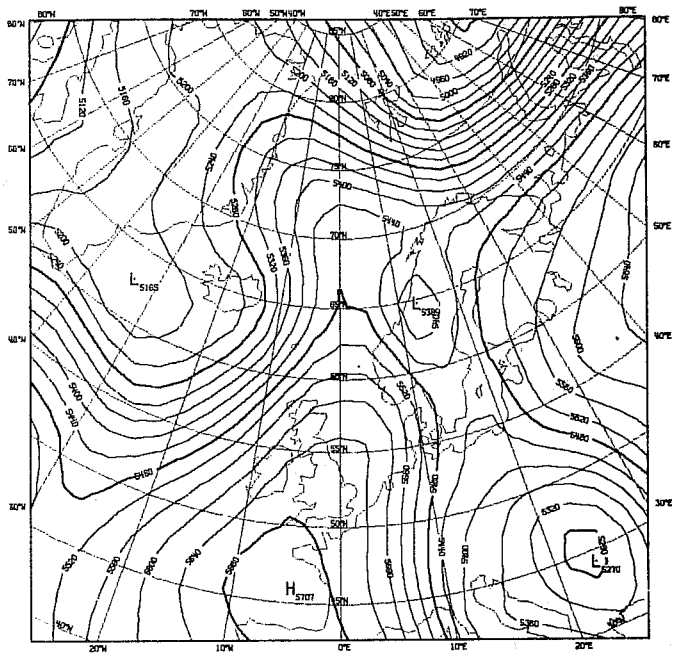

Fig. 6 As Fig. 4, however, initialised height field

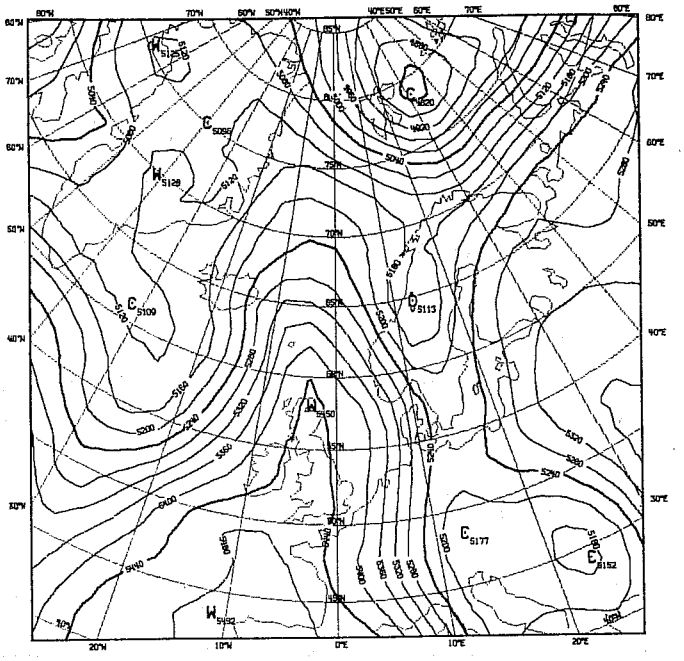

Fig. 7 Thickness of the 1000-500 mbar layer, for the initialised fields

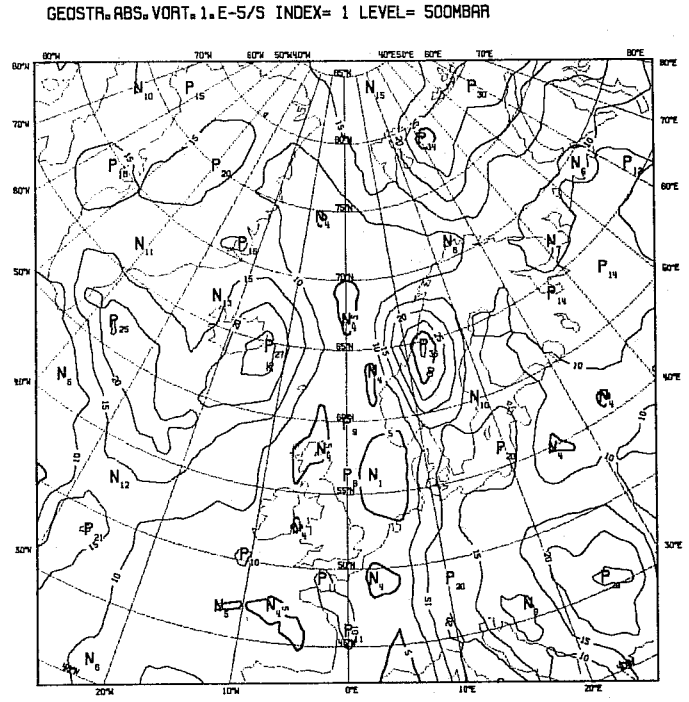

Fig. 8 The geostrophic absolute vorticity at 500 mbar for the initialised field

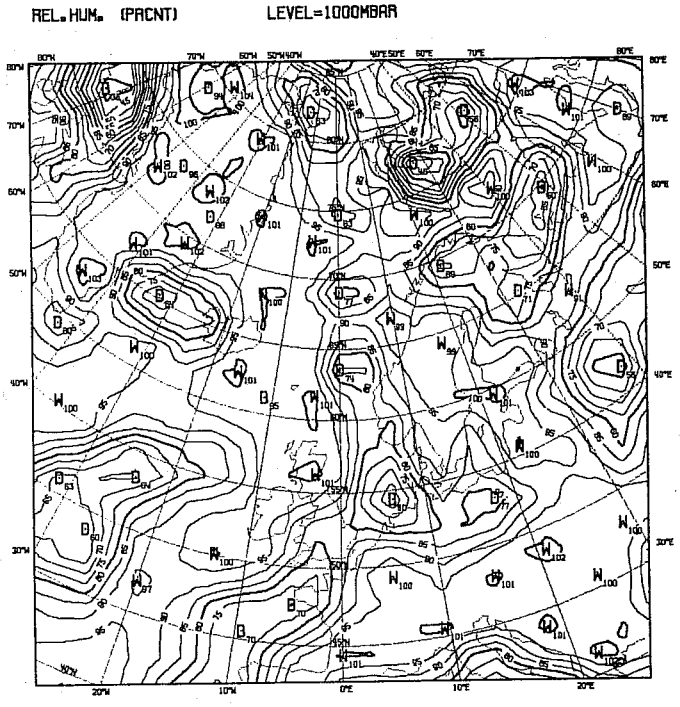

Fig. 9 Initialised relative humidity at 1000 mbar

3.2 Vertical velocities

From the first-guess, the analysis and the initialised wind fields the vertical velocity at some levels are presented. The 700 mbar results are shown in Figs. 10, 11 and 12.

The first-guess shows a strong upward motion in front of the cold front (Fig. 10). The analysis, however, fails to show such a meteorologically consistent picture (Fig. 11). The divergent part of the wind appears to be badly analysed. After the initialisation the vertical motions are reasonable again (Fig. 12). They are in general of the same order of magnitude as the first-guess vertical motions but less noisy.

The solution of the omega-equation for the three fields is shown in Figs. 13, 14 and 15, where all terms in Equations (1) to (10) have been included. Now all three fields have consistent vertical motions. From Figs. 11 and 14 it is seen that the analysed height field leads to a much better vertical velocity field than the analysed wind field. (This, of course, is the reason for deriving the omega-equation). Further it is seen that the initialised vertical motions (Fig. 12) agree with those of the omega-equation (Fig. 15), in sign order of magnitude, and overall appearance, but differences in detail occur, e.g. up to 2.4 cm/s off the Norwegian coast.

In Fig. 15 the full effect of latent heat release has been taken into account. In the initialised field, however, this effect is only present in the first-guess field and not in the initialisation procedure itself. The solution to the omega-equation, if latent heat release is put to zero, (Fig. 16) is as far as upward motions are concerned, still in somewhat better agreement with the initialised fields than the solution to the full equations.

At higher levels the difference between the initialised vertical motions and the solution to the omega-equation becomes larger. At 500 mbar the upward motion region south west of Ireland in the initialised field (Fig. 17) is not present according to the omega-equation (Fig. 18). In general the initialised vertical velocities show larger extremes than the omega-equation results. This effect is also clear at 300 mbar (Figs. 19 and 20) and at 100 mbar (Fig. 21) where the solution to the omega-equation is zero in accordance with the specified boundary conditions.

Part of the difference at higher levels will therefore be due to this boundary condition, but the 100 mbar initialised field (Fig. 21) is too noisy to be reliable, too. The forecast vertical velocity is even more noisy at this level (not shown).

The contributions of the separate terms in Equations (2) and (6) to the vertical velocity are shown in the next figures. The differential vorticity advection F_ζ induces a rather small vertical velocity (Fig. 22) as compared to the temperature advection term F_θ. The sum of these "dynamical vertical velocities" (Fig. 24) constitutes most of the vertical motion field, and only minor contributions are found from the friction (ω_f, Fig. 25) and the terrain topography (ω_t, Fig. 26). The latent heat release contribution, which is the difference of the fields shown in Figs. 15 and 16, is significant in regions with large vertical motions (Fig. 27).

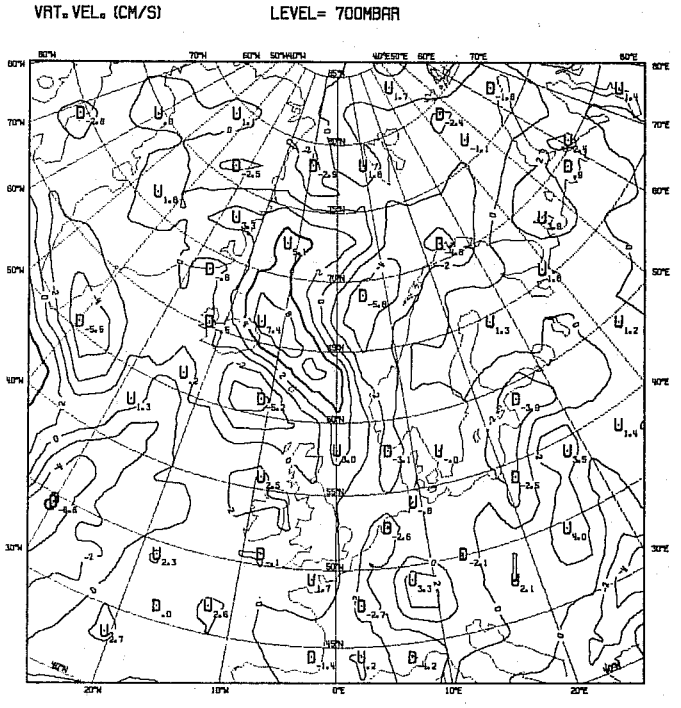

Fig. 10 Vertical velocity at 700 mbar as obtained by integrating the divergence of the first-guess horizontal wind

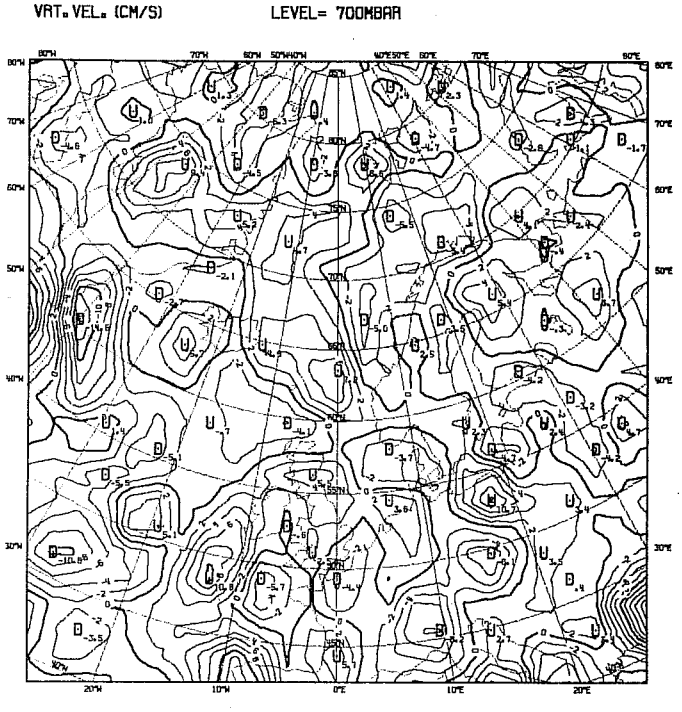

Fig. 11 As Fig. 10, however, for the analysed horizontal wind

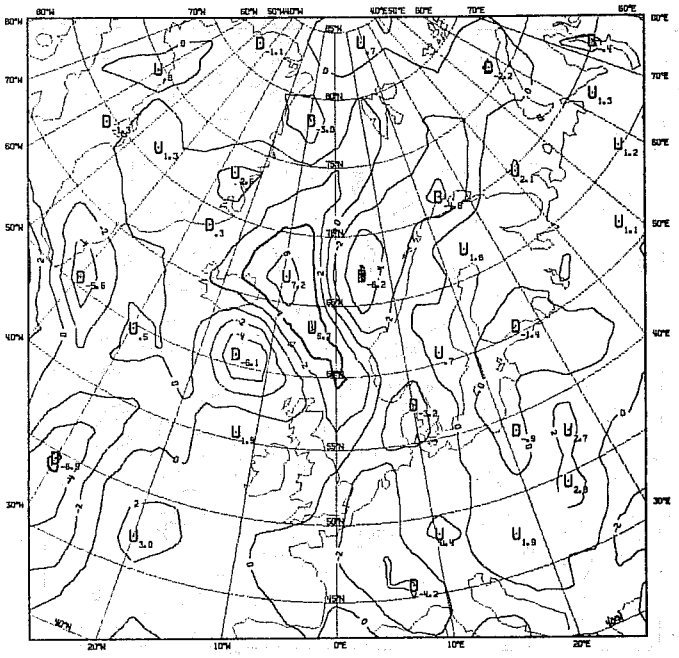

Fig. 12 As Fig. 10, however, for the initialised horizontal wind

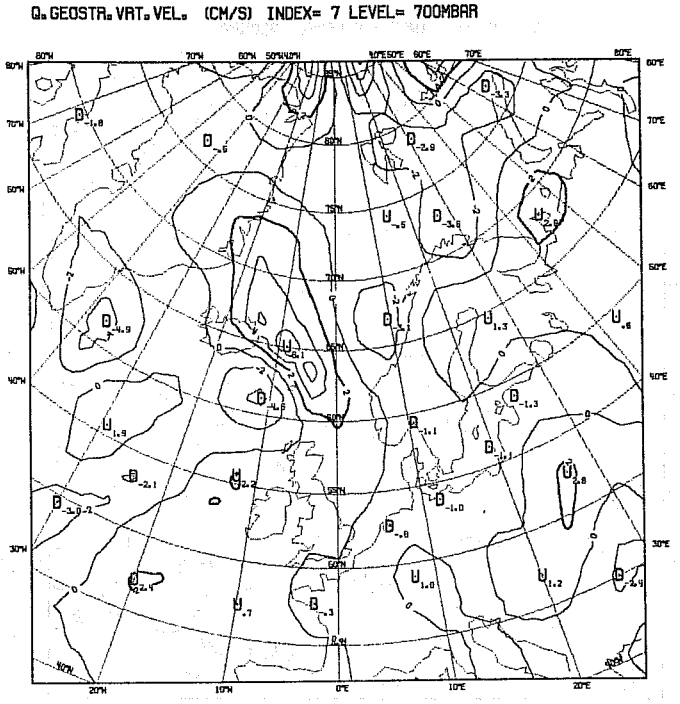

Fig. 13 Vertical velocity at 700 mb as obtained by integrating the quasi-geostrophic omega-equation using the first-guess height, temperature and relative humidity fields

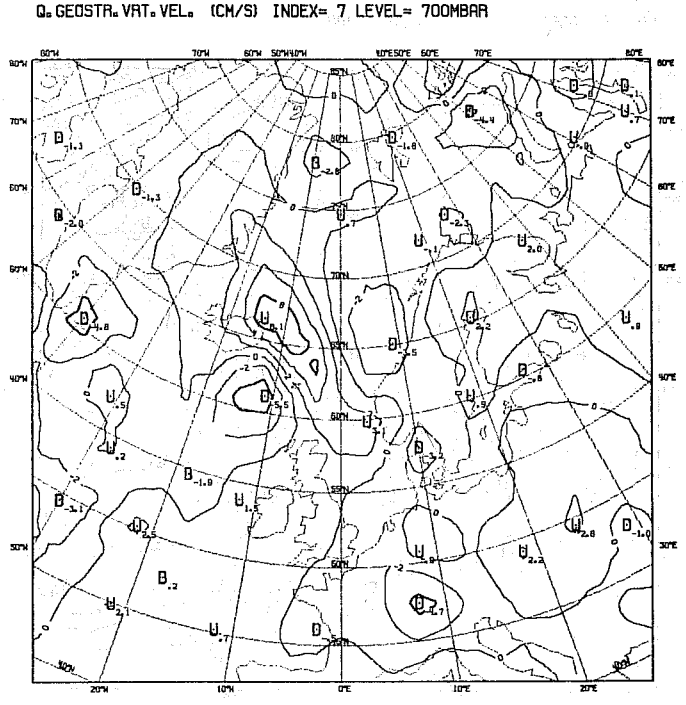

Fig. 14 As Fig. 13, however, using the analysed fields

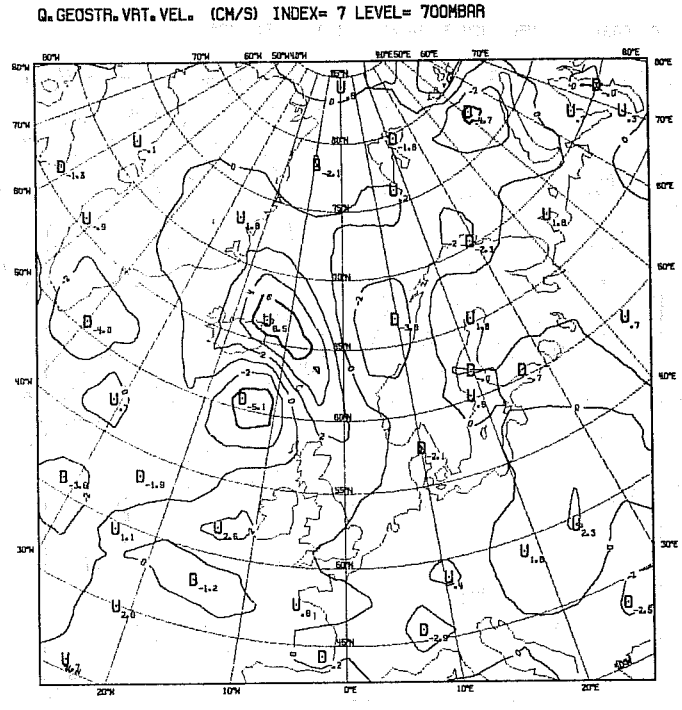

Fig. 15 As Fig. 13, however, using the initialised fields

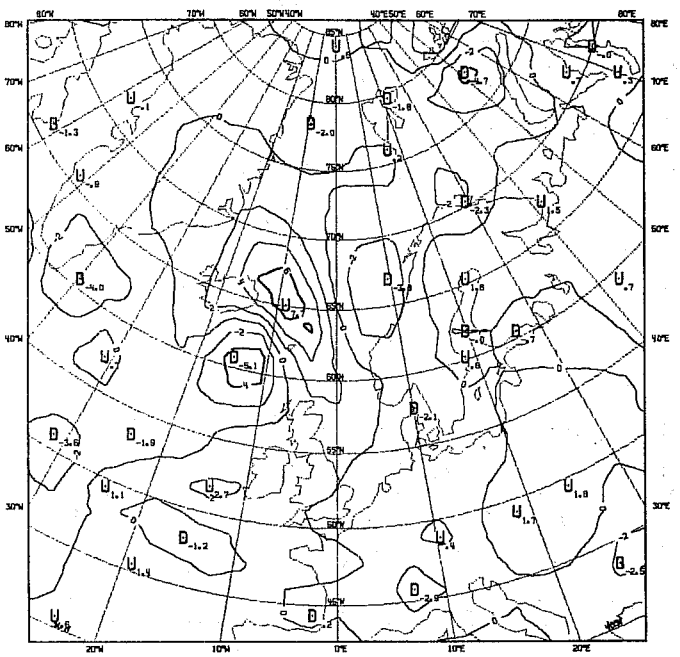

Fig. 16 As Fig. 15, but without latent heat release

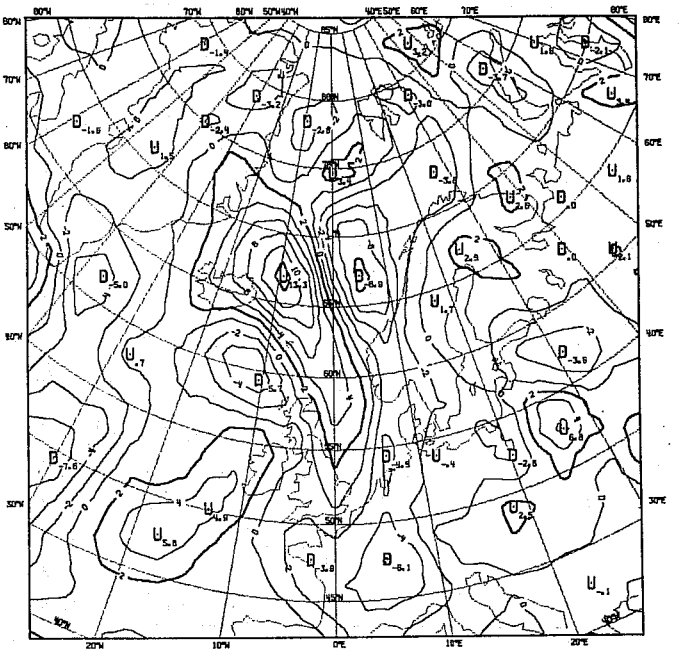

Fig. 17 As Fig. 12, however, at 500 mbar

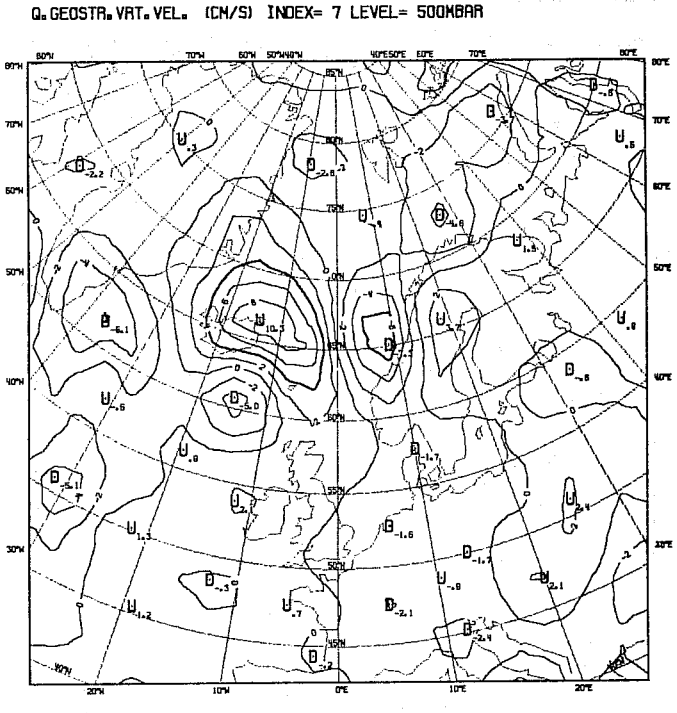

Fig. 18 As Fig. 15, but at 500 mbar

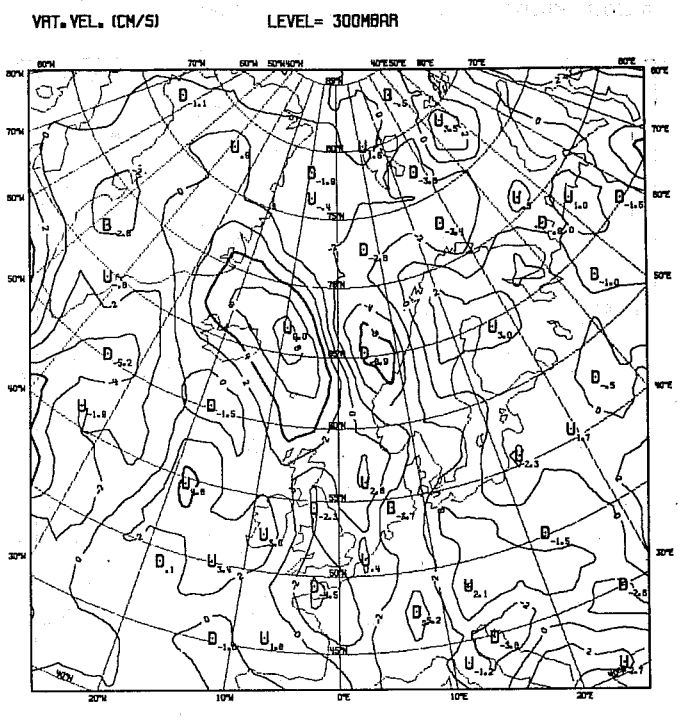

Fig. 19 As Fig. 12, but at 300 mbar

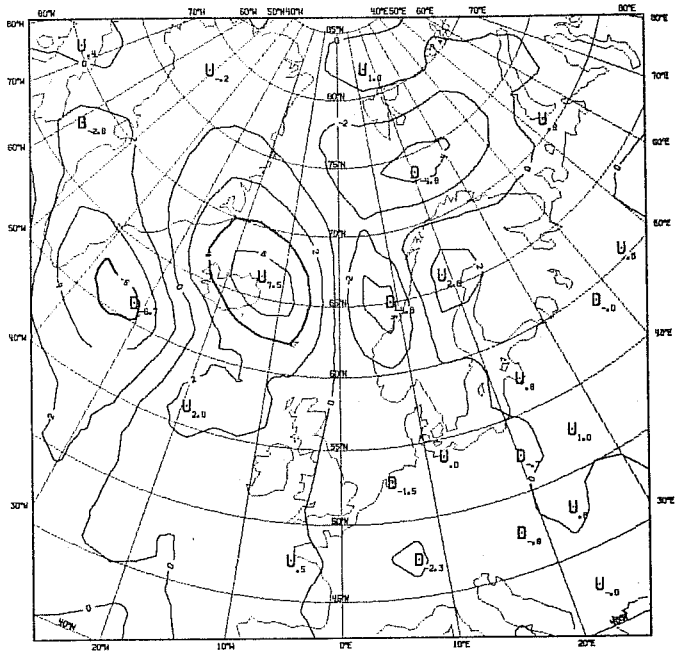

Fig. 20 As Fig. 15, but at 300 mbar

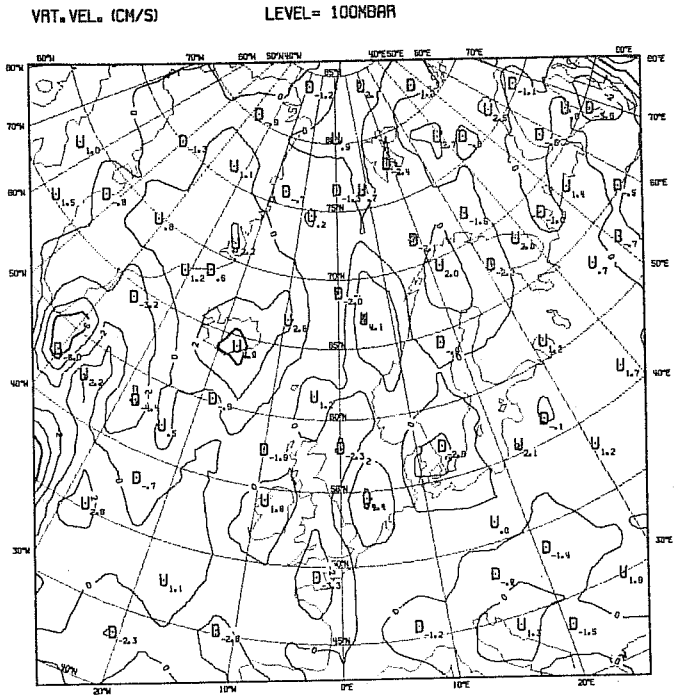

Fig. 21 As Fig. 12, but at 100 mbar

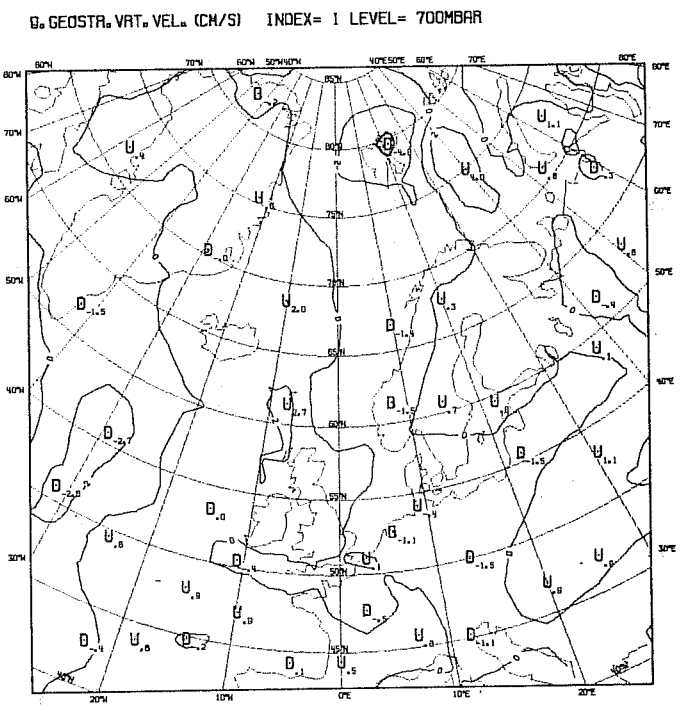

Fig. 22 As Fig. 15, but only using F_ζ (see Eq.(2)) as forcing, and putting $\omega_s=0$ (see Eq.(6))

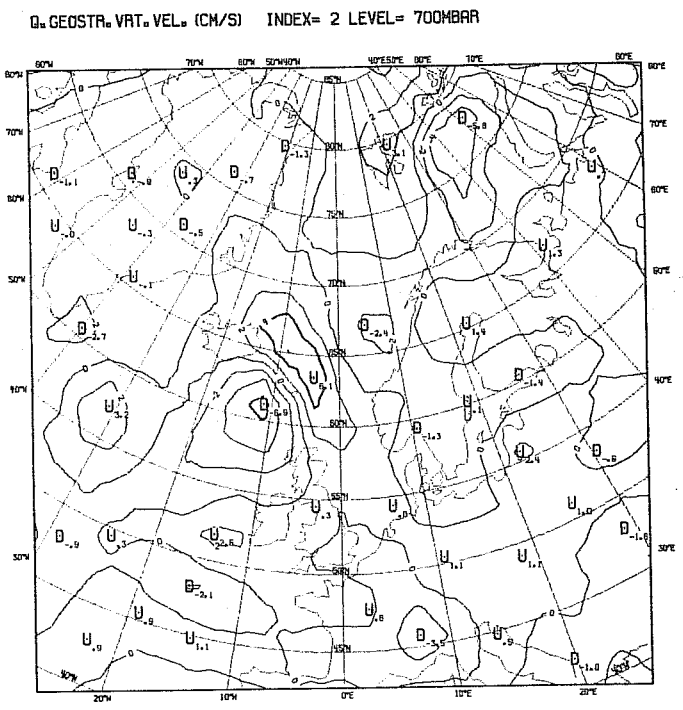

Fig. 23 As Fig. 15, but only using F_θ (see Eq.(2)) as forcing, and putting $\omega_s=0$ (see Eq.(6))

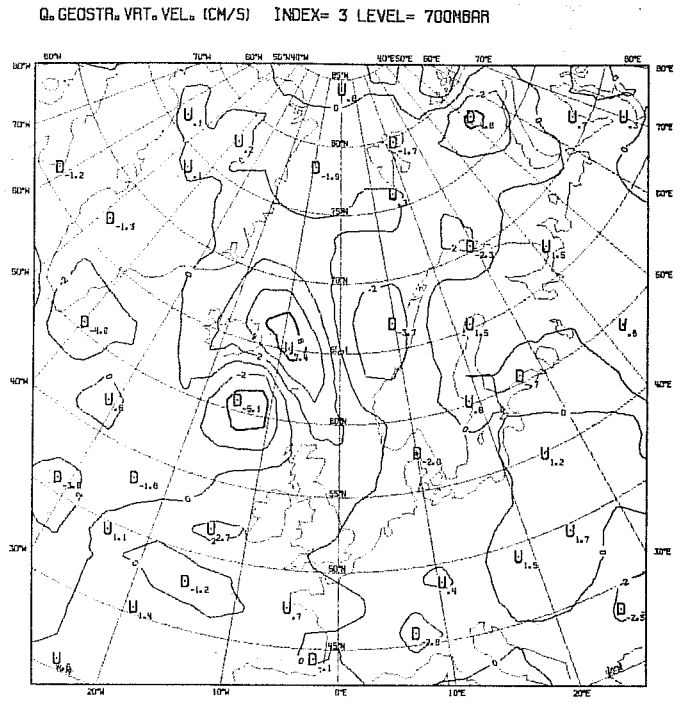

Fig. 24 As Fig. 15, but only using $F_\zeta + F_\theta$ (see Eq.(2)) as forcing, and putting $\omega_s = 0$ (see Eq.(6))

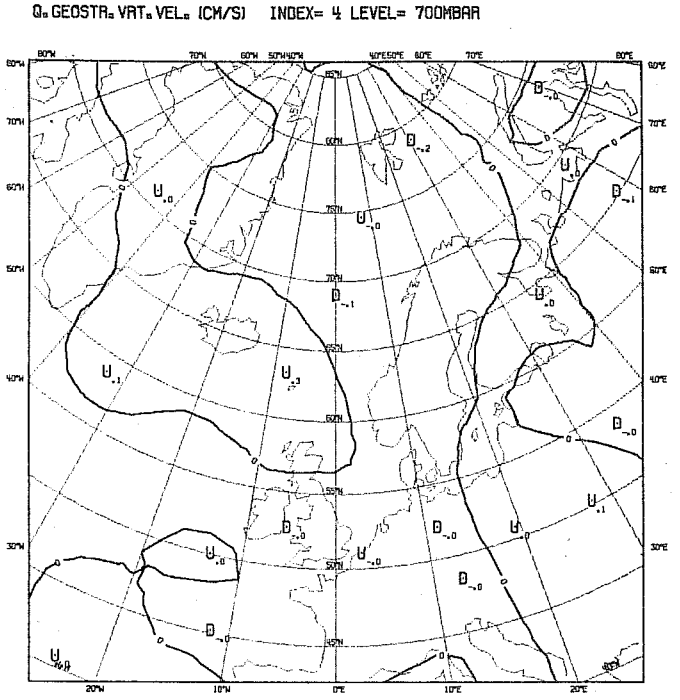

Fig. 25 The contribution of the surface friction to the vertical velocity in the situation of Fig. 15

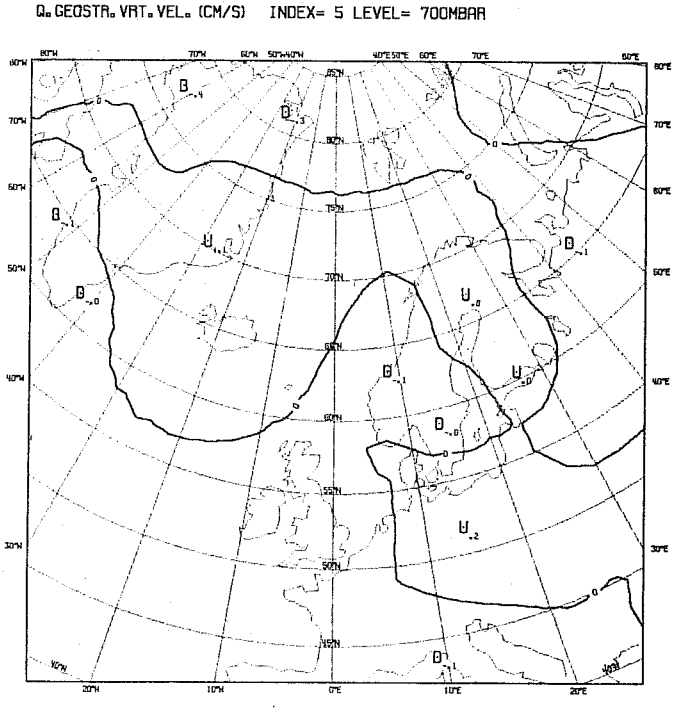

Fig. 26 The contribution of surface topography to the vertical velocity in the situation of Fig. 15.

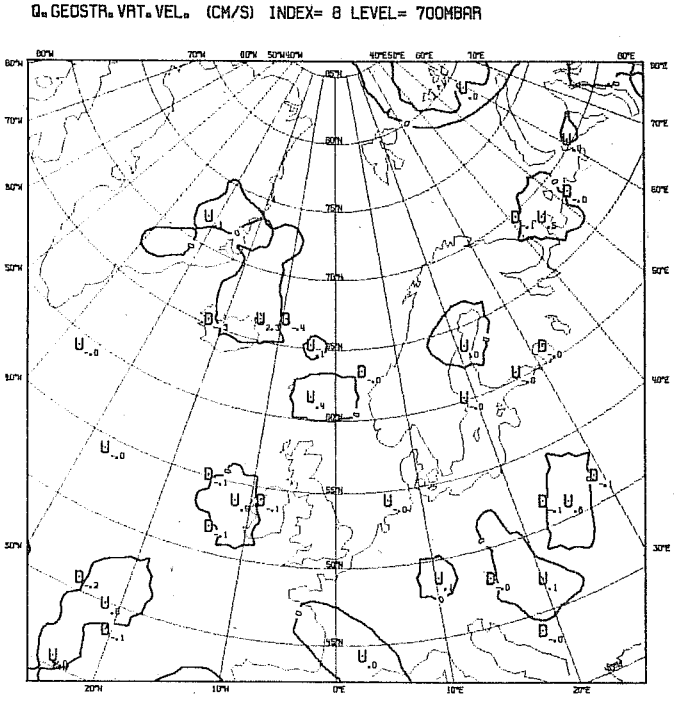

Fig. 27 The change in the vertical velocity due to latent heat release, in the situation of Fig. 15.

3.3 Tendency and precipitation ratio

To illustrate possible applications, the omega-equation tendency and large scale precipitation rate are shown in the next figures. The surface pressure tendency (Fig. 28) and the 500 mbar height tendency (Fig. 29) are small near the low pressure centre over Iceland, indicating that the system is not developing strongly. The system is seen to move north-east.

The large scale precipitation rate according to the omega-equation in the first-guess field (Fig. 30) is very high, as compared to the analysis result (Fig. 31). Because the initialisation uses the model, it is to be expected that the initialised fields lead to a precipitation rate somewhere in between the first-guess and analysis fields. This indeed is observed (Fig. 32).

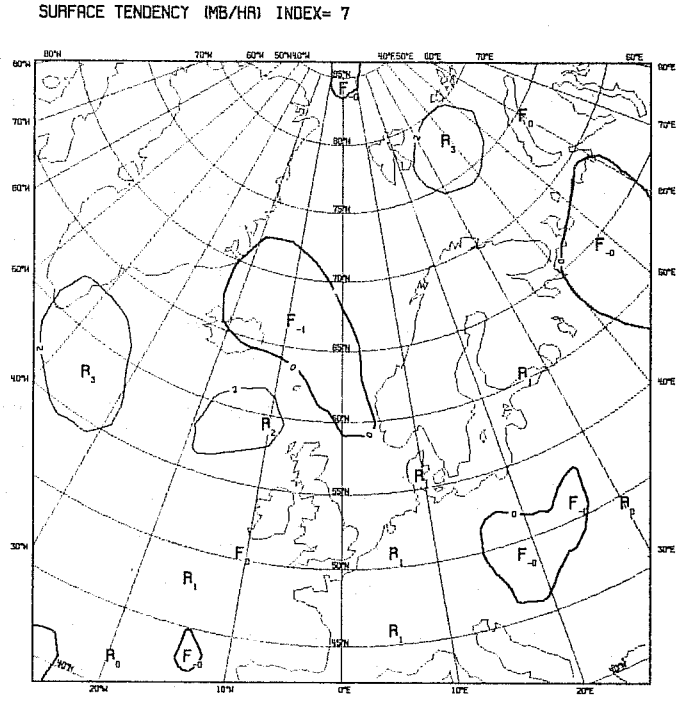

Fig. 28 The surface pressure tendency, derived using the field shown in Fig. 15

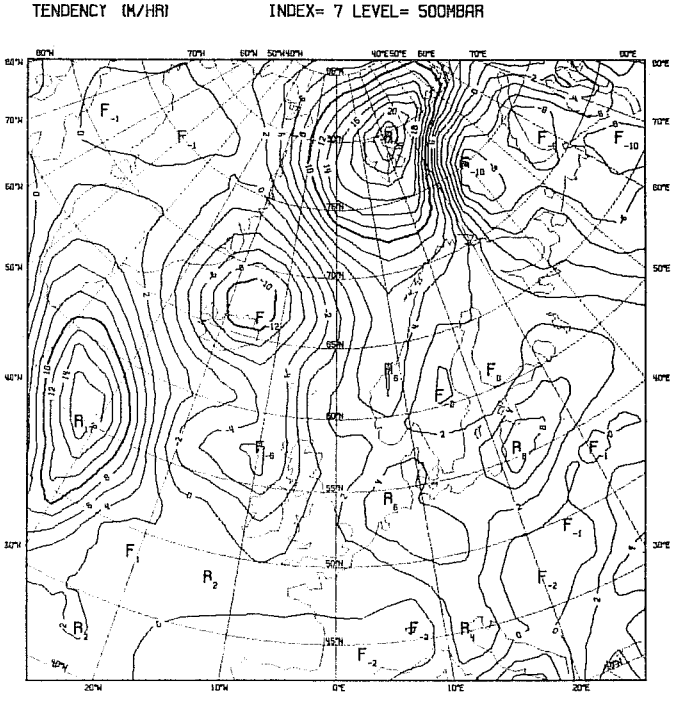

Fig. 29 The 500 mbar level height tendency, derived using the field shown in Fig. 15

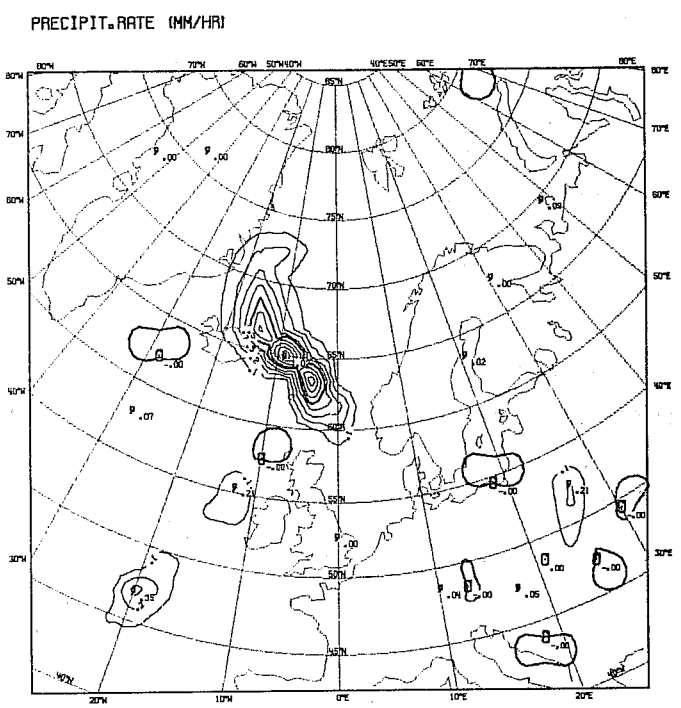

Fig. 30 The precipitation rate as derived from the first-guess fields

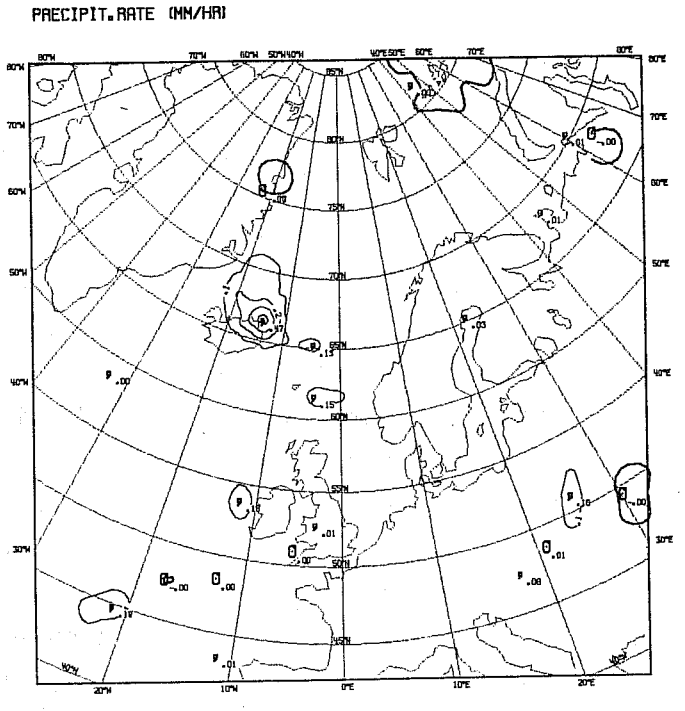

Fig. 31 The precipitation rate as derived from the analysed fields

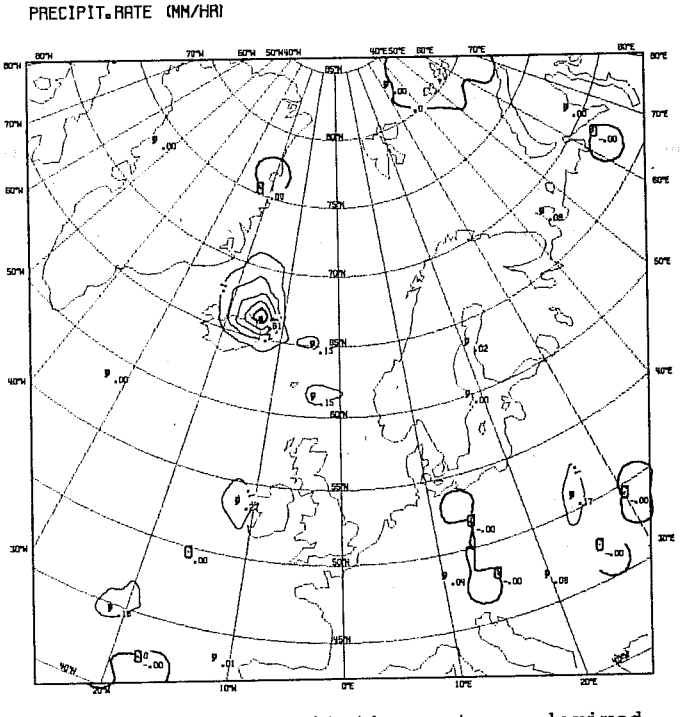

Fig. 32 The precipitation rate as derived from the initialised fields

4. CASE STUDY 2

The quasi-geostrophic diagnostic routine has been applied to the FGGE analyses of 18Z 4 December 1978. The system of interest is a classical, textbook looking extratropical cyclone developing rapidly in the extreme western Pacific northwest of the Japanese Islands. The SLP/1000-500 thickness and 500 mb height/vorticity charts are shown in Figs. 33 and 34, respectively. The principal objective of this study was to assess the vertical velocity fields provided by the ECMWF initialisation. The weather system in question is one where the quasi-geostrophic fields should be qualitatively and quantitatively quite reasonable (i.e. the storm is well defined, but not so intense that ageostrophic effects play a dominant role). Thus, the quasi-geostrophically derived quantities provide a very meaningful basis for comparison. Moreover,, the synoptic situation is one where the initialisation (or any other procedure) ought to be able to produce a reliable picture of the vertical motions. If it cannot, there is probably not much hope elsewhere. Thus, we view a favourable comparison here as a necessary (but not sufficient) condition for expecting reasonable vertical motions from the initialisation in general. As will be seen, this minimum capability by and large appears satisfied.

The initialised vertical motions at the 700, 500, and 300 mb levels are shown in Fig. 35. The corresponding fields derived geostrophically from the initialised height and moisture analyses appear in Fig. 36. These fields include all forcing (vort adv + thermal adv + friction + latent heat). The separate contributions of each are quite reasonable - that is, in accord with a priori expectations). Comparison of Figs. 35 and 36 shows that the independently computed vertical motion fields correlate rather well. Differences appear within the range of uncertainty about the true fields, except possibly the negative region at 300 mb of the initialised plot. That aspect of the initialised vertical velocities, especially when coupled with the fact it is more pronounced at 200 and 100 mb, Fig. 37, seems unrealistic (the quasi geostrophic vertical velocities are forced to zero at 100 mb). It may, however, be related in a somewhat reasonable way to detailed aspects of the circulation associated with the jet at tropopause levels (tropopause folding?); but persuit of that question will require further evaluation, for example of isentropic wind vertical cross sections.

A check on the reliability of the quasi-geostrophic vertical velocities can be obtained from comparison of the geopotential tendencies derived therefrom (via vorticity equation) and the tendencies actually observed. Fig. 36 compares the derived 1000 mb tendency (converted to SLP tendency) and the tendency field obtained by differencing the 1800 GMT 4 December analysis with that for 0000 GMT 5 December. Given that the observed tendencies apply to 2100 GMT while the diagnosed are valid at 1800, the two fields are remarkably consistent. This lends credence to the quasi-geostrophic vertical velocities, and to the extent the initialised agree, to them as well.

An important aspect of the quasi-geostrophic vertical velocities is the contribution of latent heat release. This can be seen by comparing Fig. 36 with the corresponding fields derived without the latent heating (Fig. 39). Obviously, latent heat release is crucial to completely and properly specify the vertical motion field in the quasi-geostrophic framework. Presumably, this is true for the vertical motions coming out of the initialisation. The initialisation itself knows nothing about diabatic processes, but the fields upon which the initialisation operates do. That is, the analysed winds reflect the influence of latent heat release which occurred during the 6 h forecast from the previous analysis. The relevant convective and large scale precipitation forecasts are shown in Fig. 40. Mental addition of these two fields yields a pattern which closely resembles the latent heat alone vertical motion (Fig. 41) in the quasi-geostrophic calculations. The latent heat in the quasi-geostrophic calculations is large-scale only. However, the frontal zone is saturated (Rh >80%) and the "dry" vertical motion is up, so precipitation is produced. One can reasonably infer from this that, indeed, the "physics" played an important role in the vertical motion field output by the initialisation. From the opposite perspective, given that the vertical motions are quite realistic, one can say that, in this case at least, the physics are doing a rather reasonable job.

One somewhat subtle difference between the diagnosed vs initialised vertical velocities is that the maximum upward region of the former slopes to the west somewhat more than in the latter. This may be due to the fact that the maximum of convective latent heat release of the forecast model is likely higher than the latent heating ($\approx$ 700 mb) of the diagnostics. That is, the dry processes in both diagnostics and forecast tend to produce a sloping column of rising motion, but the convective latent heating in the forecast counteracts that so the updraft slopes to a lesser extent. This and other related questions born from this case are subjects of further investigation.

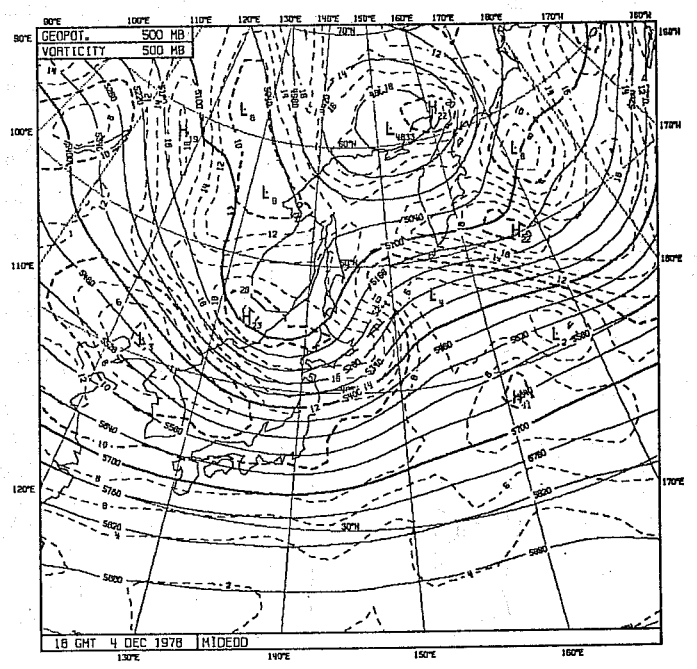

Fig. 33 Sea-level pressure (solid, mb) and 1000-500 mb thickness (dashed, m), 1800 GMT 4 Dec 1978.

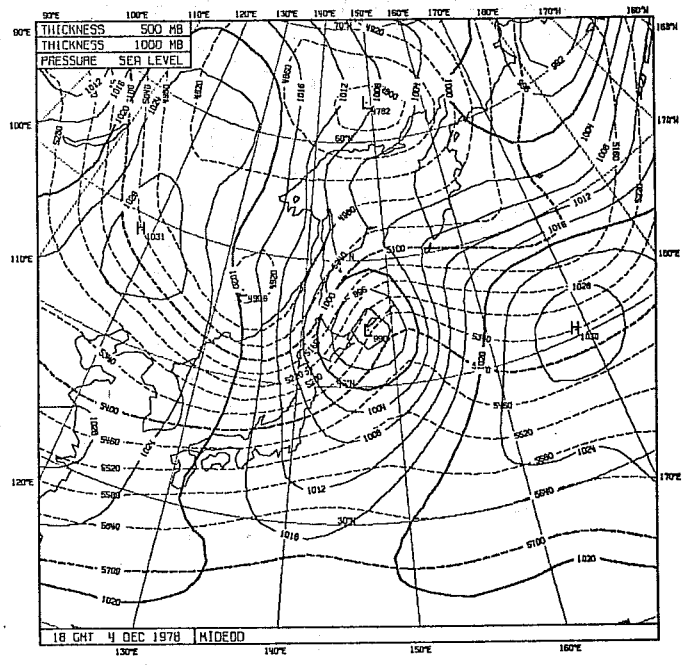

Fig. 34 500 mb height (solid, m) and 500 mb absolute vorticity (dashed, $10^5 s^{-1}$), 1800 GMT 4 Dec 1978

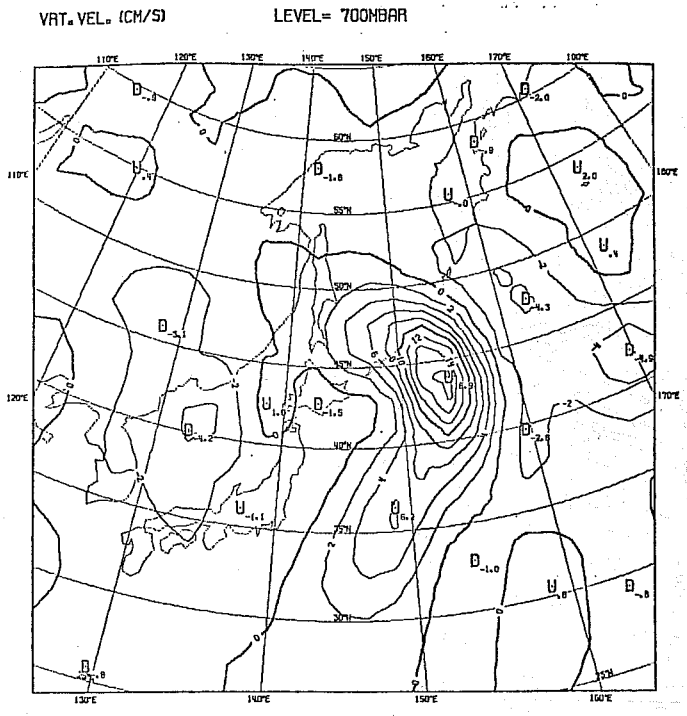

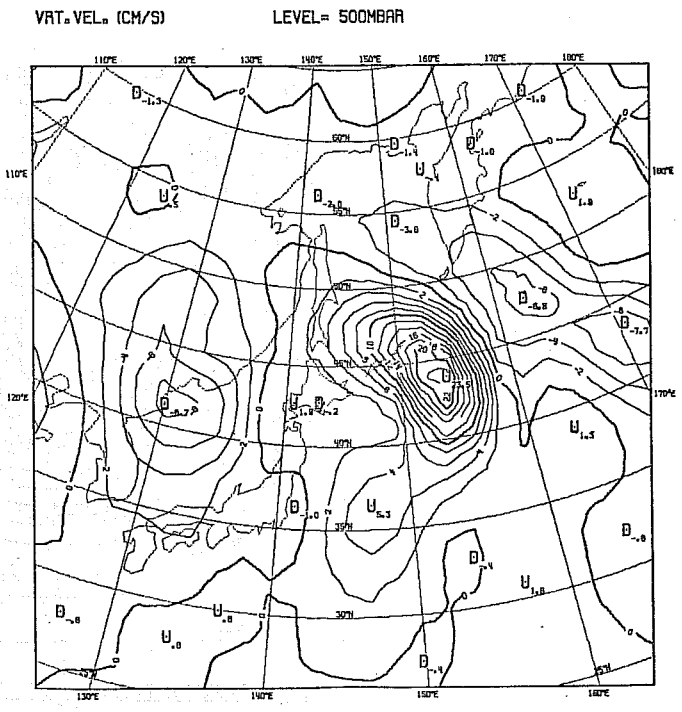

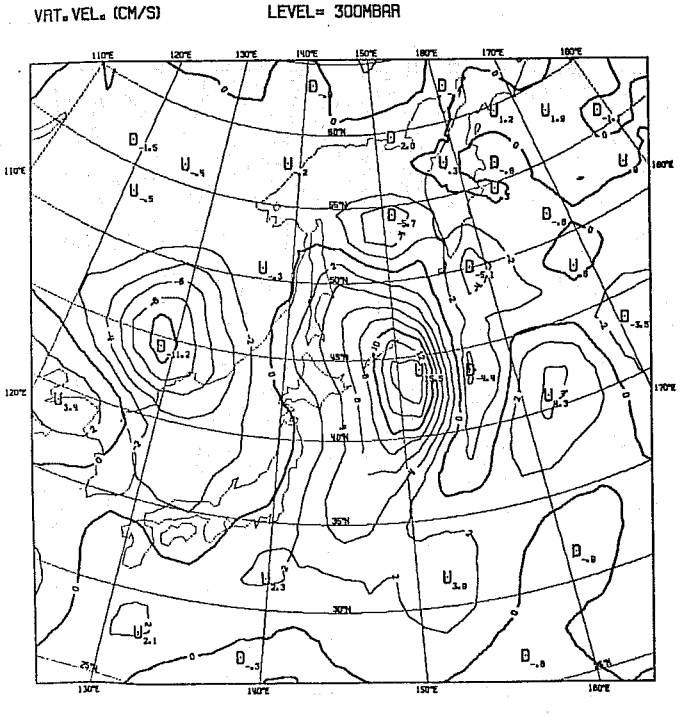

Fig. 35 700(a), 500(b), and 300 mb(c) initialized vertical velocities, 1800 GMT 4 Dec 1978. Units: cms^{-1}

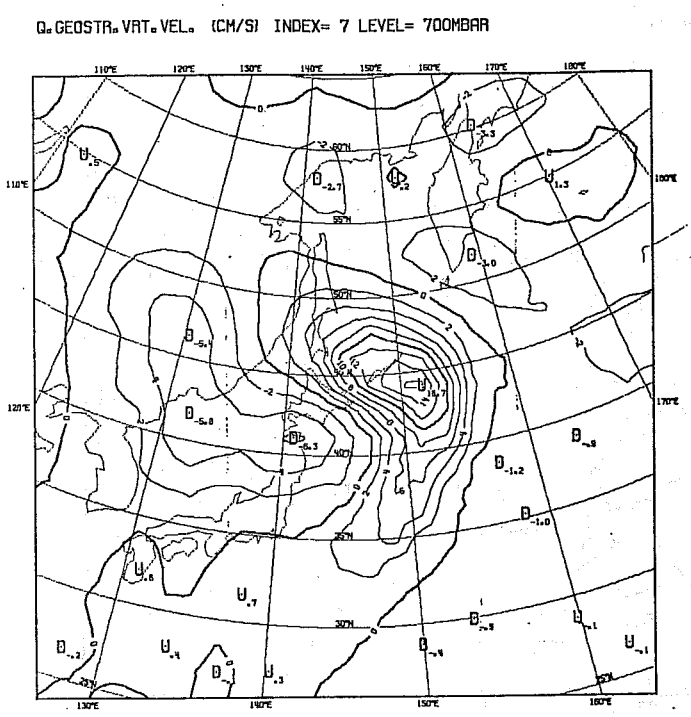

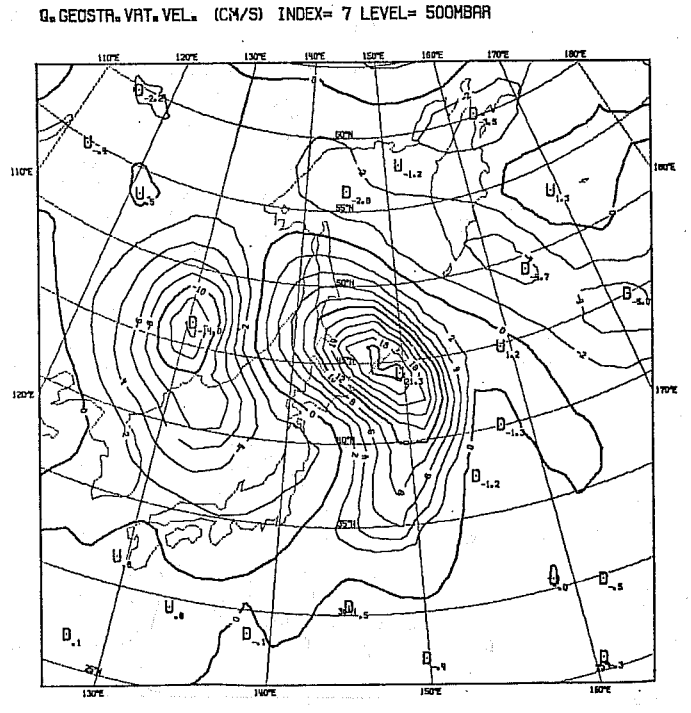

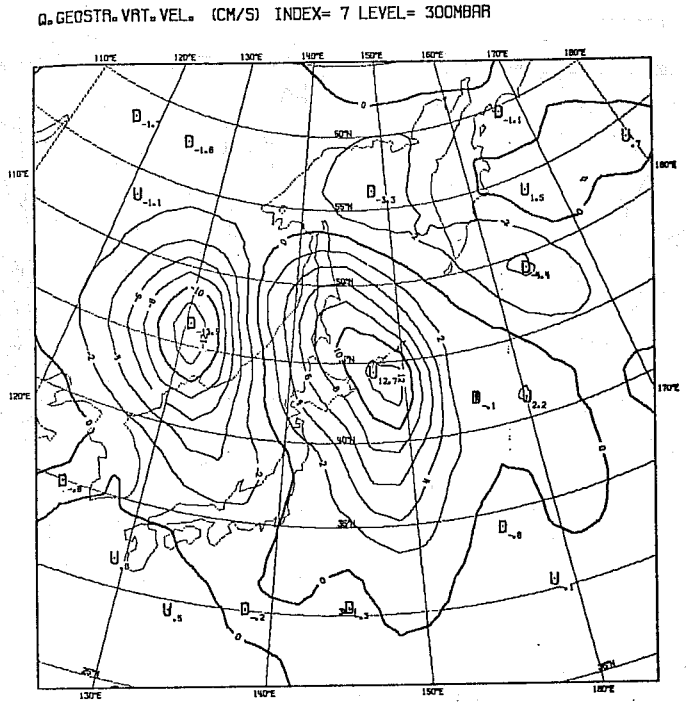

Fig. 36 700(a), 500(b), and 300 mb(c) quasi-geostrophic vertical velocities, 1800 GMT 4 Dec. 1978. Units: cms^{-1}

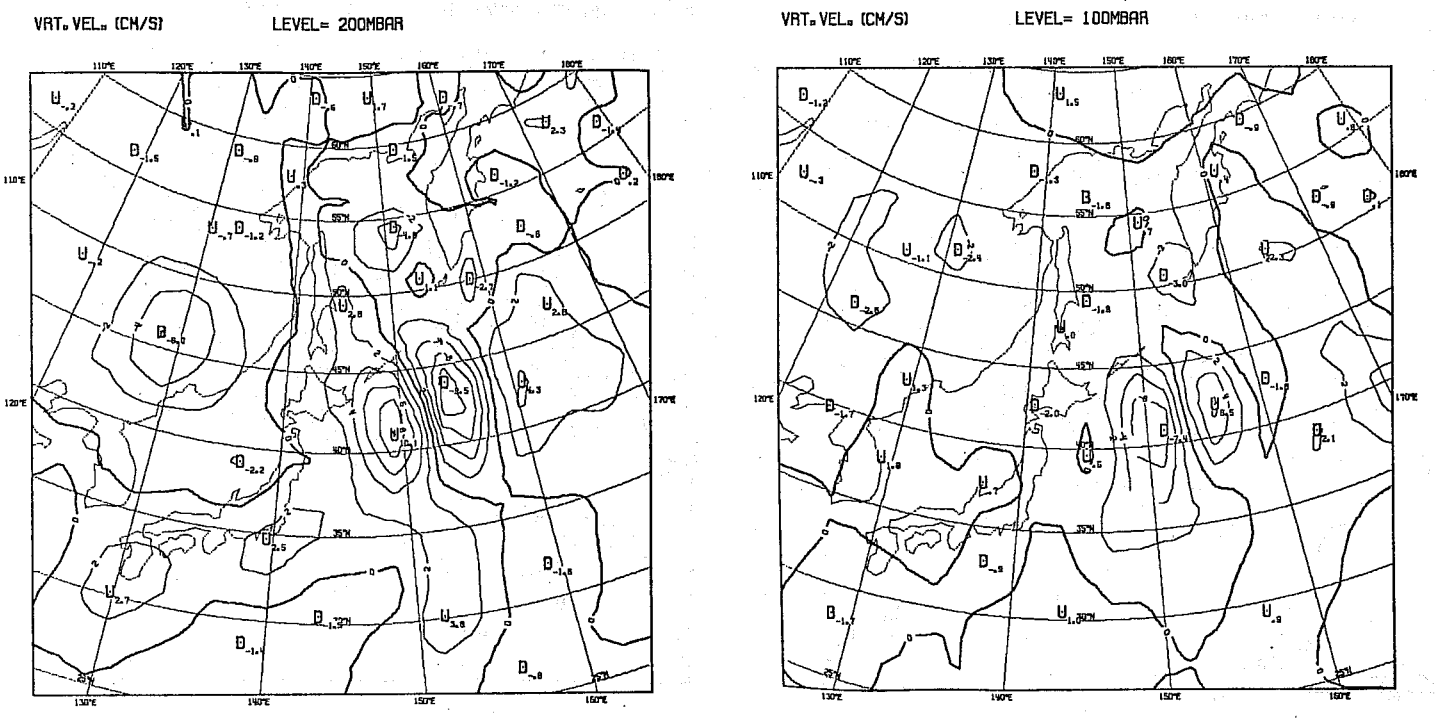

Fig. 37 200(a) and 100(b) initialised vertical velocities, 1800 GMT 4 Dec 1978. Units: cms^{-1}

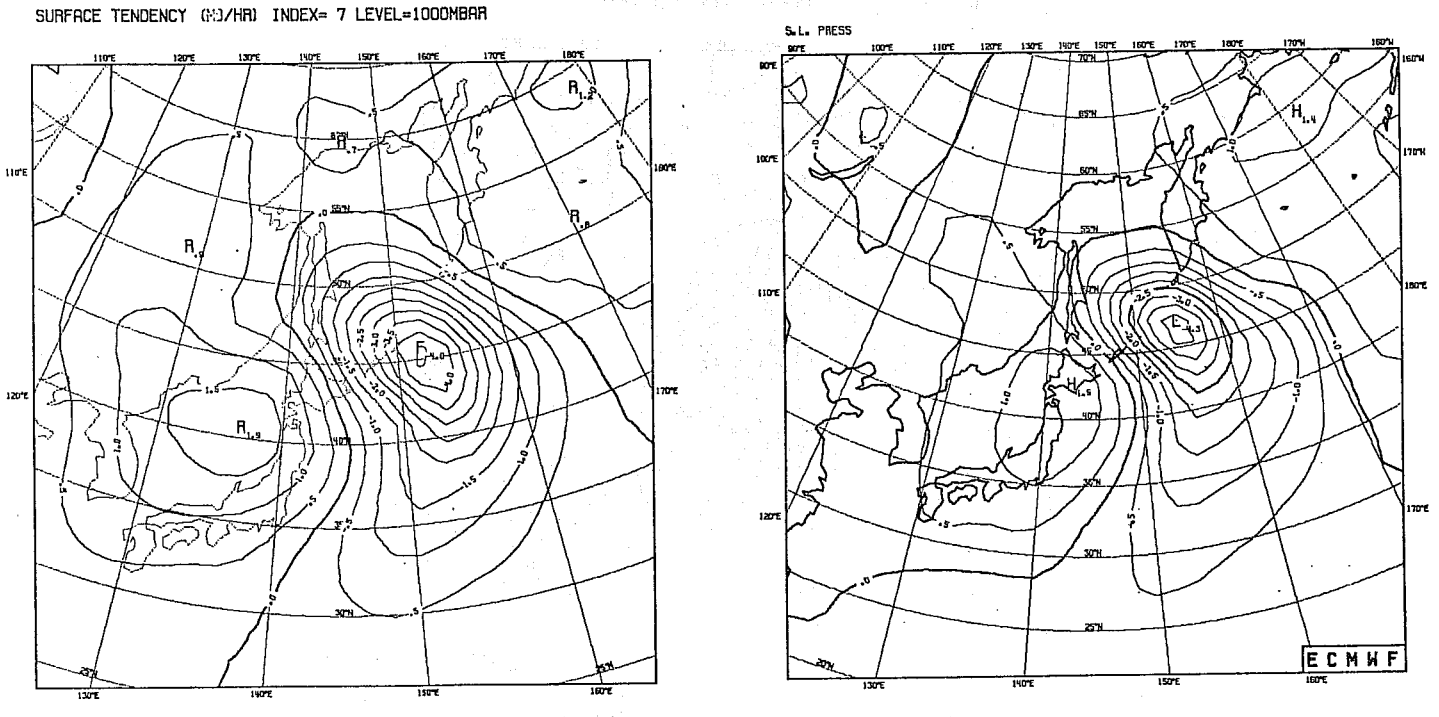

Fig. 38 Quasi-geostrophic (a) 1800 GMT 4 Dec 1978, and observed (b) sea-level pressure tendency (mb h^{-1}). Observed is obtained from 0000 GMT 5 Dec and 1800 GMT 4 Dec SLP analyses.

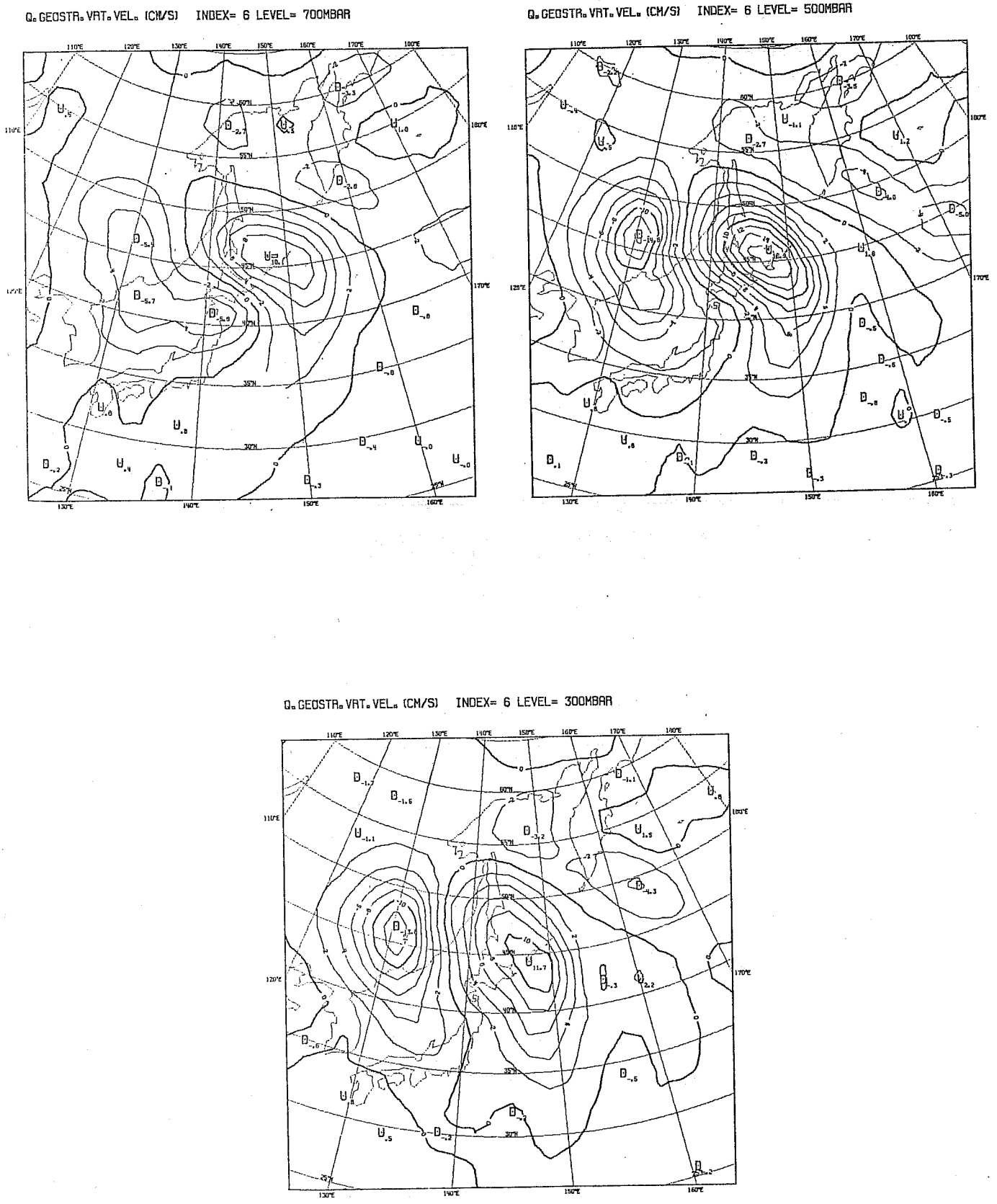

Fig. 39 700(a) 500(b) and 300 mb(c) quasi geostrophic vertical velocities, 1800 GMT 4 Dec 1978. Units: cms^{-1}

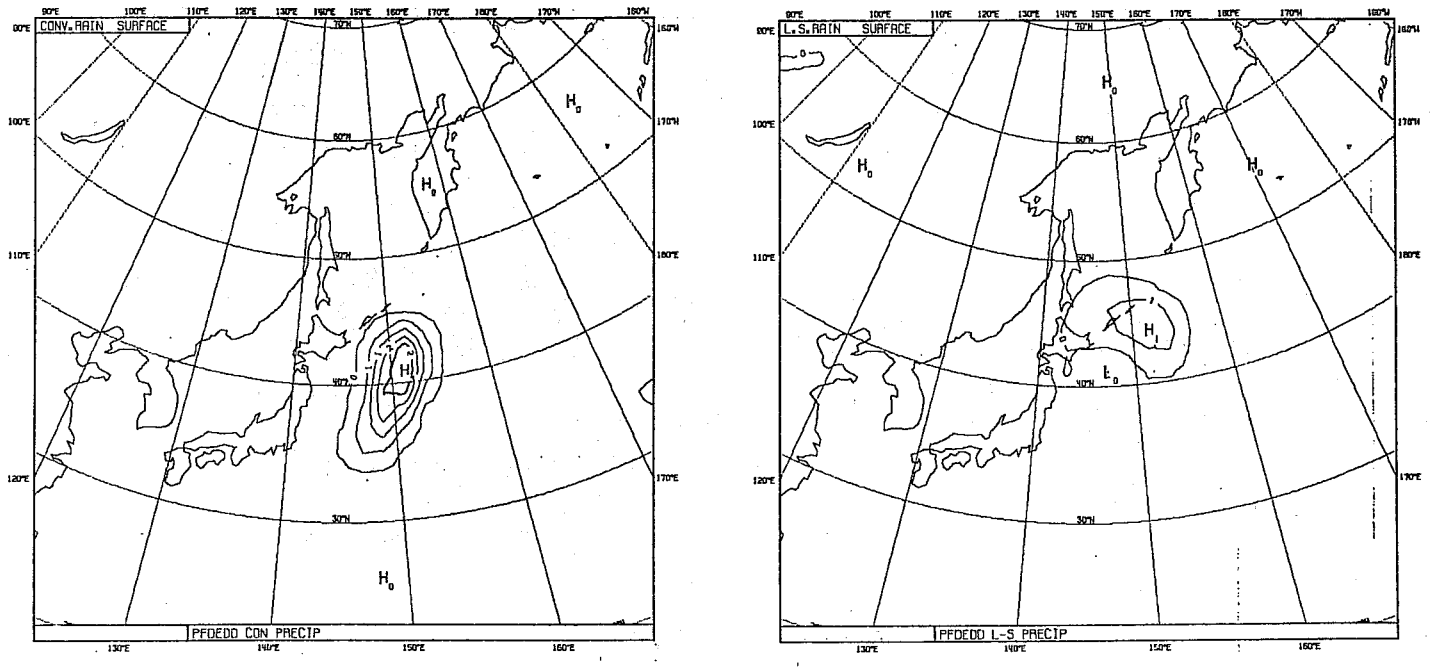

Fig. 40 Convective (a) and large-scale (b) precipitation (10^{-1} in h^{-1}) of 6 h forecast from 1200 GMT 4 Dec 1978

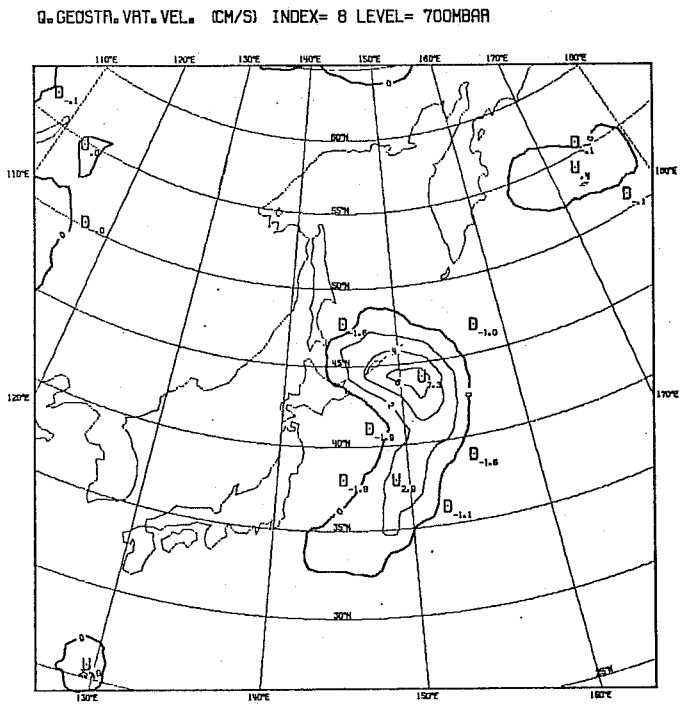

Fig. 41 700 mb quasi-geostrophic vertical velocities due to latent heat release, 1800 GMT 4 Dec 1978. Units: cms^{-1}

5. CONCLUSIONS

For two cases the vertical velocity obtained from the divergence of the horizontal wind field has been compared with the solution to the omega-equation over the Northern Atlantic. For levels not too high in the atmosphere a good agreement has been found for the forecast field (which affirms the assumptions made in the derivation of the quasi-geostrophic omega-equation). In the analysis field, however, the horizontal wind divergence is completely wrong (which has been the motivation for deriving the omega-equation). After initialisation the divergence of the horizontal wind field leads to consistent estimates of the vertical motions. The initialisation procedure achieves this by changing both height and wind fields. Because the initialised horizontal wind field leads to the same order of magnitude vertical motions as the omega-equation applied to the analysis field, it is concluded that the initialisation procedure mainly adjusts the horizontal wind divergence, and only brings about relatively small changes in the height fields.

At the higher levels (pressure less than 300 mbar) the vertical velocity field from the initialisation displays an excessive amount of noise. The presented solution of the omega-equation is not reliable in these regions, either, because of boundary effects.

It is stressed that the above conclusions are based on two test cases only, and may have to be revised after a more thorough study. This is especially true, since several errors are known to have existed in the used version of the data assimilation system. This is also the reason that some interesting features have not been studied into more detail yet. These are the noise in the forecast and initialised vertical velocity at high levels and the large difference between forecast, analysed and initialised precipitation rate.

Another future study will look into the vertical velocity fields obtained after the first iteration step in the initialisation. Leith (1979) indicated that these should almost coincide with the omega-equation results.

References

Holton, J.R., 1972: An Introduction to Dynamic Meteorology, Academic Press, New York

Leith, C.E., 1979: Nonlinear normal mode initialisation and quasi-geostrophic theory. NCAR ms. 0901-79-01.

Temperton, C., and D.L. Williamson, 1979: Normal Mode Initialisation for a Multi-level Gridpoint Model. ECMWF Technical Report No. 11.

Tracton, M.S., 1978: Diagnosis of Numerical Analyses and Forecasts from the Perspective of Quasi-Geostrophic Dynamics. NMC Office note 183.

APPENDIX

THE COMPUTER PROGRAMS FOR THE SOLUTION OF THE OMEGA-EQUATION AT ECMWF

1. GENERAL DESCRIPTION

The suite to solve the omega-equation start with a Cyber program to read the input data (height, temperature and relative humidity fields at the mandatory levels) and a selection of other fields, such as vertical velocity, from a standard first-guess, analysis or initialised data file. It further obtains the surface topography as used in the N48 model. This program then starts a Cyber program to plot a selection of the read fields and a Cray program to solve the omega-equation. The Cray program calculates the vertical velocity according to the omega-equation, the pressure and height tendency and energy transformation. It then submits a third Cyber program (the third in the suite and actually the same as the second) to plot a selection of the results.

2. REQUIRED INPUT

The first program in the suite is the only to require input data. Three cards have to be supplied. These cards contain respectively,

1. The permanent file name of the file containing the first-guess, analysis or initialised input data in A40 format. The file must be in standard pressure coordinate format.

2. The additional text required to "ATTACH" this file (up to 80 characters, e.g. ID =).

3. The parameters to specify the area to be plotted (in free format). The parameters are:

   IAREA, 1 for the northern and 2 for the southern hemisphere

   VERT the longitude in degrees to be plotted vertically

   GL The grid distance true at 60^{o} north or south in metres

   XP, and YP : the pole coordinates.

The contents of these cards are passed through to each subsequent program in the suite including comments of the first and second card. They are printed and/or plotted by each program.

3. AVAILABILITY

The series of job control cards has been stored as the deck OMGAEQ on the Cyber update library JOBLIB,ID=DAZ with *=/. All relevant Fortran codes are kept on the Cyber update library OMEGAEQ,IP=DAN.

4. SELECTION OF THE OUTPUT PLOTS

Only few efforts have been undertaken to make the described suite generally applicable. Therefore a user will probably want to change some parts of the program. It is expected that often the desired changes relate to the selection of the plotted fields. In this Section it will be indicated how to select these fields.

Both the first Cyber program and the subsequent Cray program write one record for each required plot to a file which is used as an input by the plotting programs. The record is written by the sub routine GRDPRT, and each call to GRDPRT therefore leads to one plot.

In the Cyber program, GRDPRT is called in the subroutine READH. This subroutine reads the input (first-guess, analysis, or initialised) file and selects the fields to be used by the omega-equation solution program and the fields to be plotted. In the Cray program GRDPRT is called in the subroutines SLVOM1 (to solve the omega-equation without latent heat release) and SLVOM7 (latent heat release included). The selection of the plotted fields is done by editing these procedures.